Surface polaritons in a circularly cylindrical interface: Surface plasmons

C. A. Pfeiffer and E. N. Economou
Department of Physics, University of Virginia, Charlottesville, Virginia 22901

K. L. Ngai
Naval Research Laboratory, Washington, D. C. 20375

(Received 19 February 1974)

A theoretical investigation of surface polaritons in the circularly cylindrical geometry is presented. The complete set of Maxwell's equations (retardation effects are not neglected) is solved with the simple dielectric function, $\epsilon(\omega) = 1 - \omega_p^2/\omega^2$, where ω_p is the bulk plasma frequency. The resulting transcendental equation for the eigenfrequencies is solved via numerical methods for three representative values of the cylindricality constant, $\alpha = \omega_p a/c$, where a is the cylinder radius and c the velocity of light. In addition to the real nonradiative surface plasmons, various virtual radiative surface plasmons exist with properties depending rather strongly on α. The results are compared with existing experimental data. Further experiments are proposed in order to reveal the most interesting features of the surface plasma modes.

I. INTRODUCTION

Plasma oscillations, i.e., the collective motions of an electron gas, are an inherent property of solid-state plasmas. A nonzero local charge density in a metal or semiconductor, whose conduction electrons form an electron gas, creates long-range Coulomb fields which organize the system into collective motion. The condition, $\nabla \cdot \vec{E} \neq 0$ in the bulk material, where $\vec{E}$ is the electric field in the bulk, gives rise to one set of plasma oscillations, commonly known as the bulk plasma modes, which are characterized by the plasma frequency $\omega_p = (4\pi ne^2/m)^{1/2}$, where m and e are the electronic mass and charge and n is the electron density. The bulk plasma modes exist alone in the idealized situation where the system is unbounded by surfaces.

However, the presence of surfaces complicates the situation. Not only are the bulk plasma modes modified but new modes are created, called surface modes, which are absent in the bulk. These surface modes have properties and dispersion relations, differing from the bulk plasma modes and varying according to the characteristics of the surfaces. As with the bulk modes, the surface modes can be excited by incident electrons or photons, and, in fact, have been detected experimentally in three different geometries—the planar, the spherical, and the cylindrical geometries. There has been, to date, extensive theoretical and experimental investigation of the planar[1-5] and, to a lesser degree, the spherical[6] geometries, leading to predictions and properties which have been verified and well understood. However, there has been limited work in the cylindrical case. Englman and Ruppin[7] have considered the problem of surface optical (SO) phonons in ionic crystals of cylindrical shape; the general theory for the behavior of the modes as well as dispersion curves for the nonradiative modes have been presented. An optical experiment to excite surface plasmons (SP) was performed on Al cylinders by Miziumski[8] (these will be shown to be virtual radiative SP in Sec. IV). Ngai and Economou[9] have discussed the validity of the electrostatic approximation to the real nonradiative SP of a cylinder. These latter modes have been investigated by Ashley and Emerson[10] and dispersion curves have been included.

The solution of the complete set of Maxwell's equations in the planar and spherical geometries [with the condition that $\nabla \cdot \vec{E} = 0$ in the bulk, which gives rise to the surface plasma oscillations (SPO) alone] leads to electromagnetic fields at the surfaces with either $E_\perp$ or $H_\perp$ zero, where $E_\perp$ and $H_\perp$ are the normal components of the electric and magnetic fields at the surfaces. Thus the plane and the sphere allow pure magnetic waves (TE waves) and pure electric waves (TM waves) as the two independent solutions of the Maxwell equations.[5,11] After applying the well-known boundary conditions for the fields to the pure electric wave solution (since this solution permits the existence of surface charge and, consequently, SPO), a transcendental equation is obtained which can usually be solved for the dispersion relations of the surface plasma modes in each geometry. However, the cylindrical geometry does not allow this separation and the eigenmodes with $\nabla \cdot \vec{E} = 0$ in the bulk are superpositions of electric and magnetic waves (except for the modes without any angular dependence).[5,7,11] The cylindrical natural modes have both the perpendicular and the parallel field components coupled together. Upon application of the boundary conditions, a rather complicated transcendental equation for the dispersion relations

arises.[5,7,10,11]

Reasons exist for theoretical and experimental investigation of the surface modes in the cylindrical geometry. The latter is a geometry intermediate between the planar and the spherical and, thus, the surface modes should contain the characteristics of the other two geometries; yet, partly because of the coupling of the normal and parallel field components, these modes will have their own distinct properties. Moreover, the cylindrical geometry is open to more varied experiments which can better reveal not only the properties of the surface modes but also the nature of the materials used. A case which will be discussed in more detail in Sec. V is the application of a static magnetic field H_0 along the axis of a cylindrical conductor such that incident electrons of mass m and charge e will spiral about the cylinder with frequency $\omega_0 = eH_0/mc$, creating thus external fields which can be Fourier analyzed to a fundamental ω_0 and to higher harmonics $n\omega_0$. Thus, by varying the field H_0, a resonant excitation of radiative surface plasmons may be achieved providing a promising source of radiation.

The purpose of this paper is thus the investigation of SPO in the cylindrical geometry. In Sec. II, the complete set of Maxwell's equations (retardation effects are not neglected) is solved with the condition, $\nabla \cdot \vec{E} = 0$ in the bulk, and the transcendental equation is obtained. Using a simple dielectric function of the form $\epsilon(\omega) = 1 - \omega_p^2/\omega^2$ for the conductor, where ω_p is the bulk plasma frequency, we solved the transcendental equation numerically for the dispersion relations of the surface modes for three representative values of the constant, $\alpha = \omega_p a/c$, where a is the radius of the cylinder; a description of the numerical techniques and the results are presented in Sec. III. The only reported experimental study of SPO in cylinders is discussed in Sec. IV in the light of the findings of Sec. III. Possible future investigation is discussed and a summary is given in Sec. V. Finally, the Appendix contains an analytical study of the behavior of the surface modes in the vicinity of the photon line.

II. THEORY

The system under consideration is a circularly cylindrical conductor of radius a imbedded in a dielectric of infinite extent, with the cylinder axis along the z axis. The conductor is characterized by a dielectric function $\epsilon_C(\omega)$, while the dielectric is characterized by $\epsilon_D(\omega)$.

As noted previously, the cylindrical eigenmodes are superpositions of electric- and magnetic-type waves. The components of the electromagnetic field for the nth mode are given by[11]

$$
\begin{aligned}
E_r &= \left(\frac{ik_z}{K_j} Z_n^{j\prime}(K_j r) a_n^j - \frac{\mu_j \omega n}{K_j^2 r} Z_n^j(K_j r) b_n^j\right) S_n \,, \\
E_\theta &= -\left(\frac{nk_z}{K_j^2 r} Z_n^j(K_j r) a_n^j - \frac{i\mu_j \omega}{K_j} Z_n^{j\prime}(K_j r) b_n^j\right) S_n \,, \\
E_z &= [Z_n^j(K_j r) a_n^j] S_n \,, \qquad (2.1) \\
H_r &= \left(\frac{n(K_j^2 + k_z^2)}{\mu_j \omega K_j^2 r} Z_n^j(K_j r) a_n^j + \frac{ik_z}{K_j} Z_n^{j\prime}(K_j r) b_n^j\right) S_n \,, \\
H_\theta &= \left(\frac{i(K_j^2 + k_z^2)}{\mu_j \omega K_j} Z_n^{j\prime}(K_j r) a_n^j - \frac{nk_z}{K_j^2 r} Z_n^j(K_j r) b_n^j\right) S_n \,, \\
H_z &= [Z_n^j(K_j r) b_n^j] S_n \,,
\end{aligned}
$$

where $j = C$ denotes the components inside the cylinder, $r < a$, and $j = D$, those outside the cylinder, $r > a$, such that $Z_n^C(x) \equiv J_n(x)$, the Bessel function of order n, $Z_n^D(x) \equiv H_n^{(1)}(x)$, the Hankel function of the first kind of order n, and the prime denotes differentiation with respect to the argument $x \equiv K_j r$. The Bessel and Hankel functions, $J_n(x)$ and $H_n^{(1)}(x)$, insure that the field components are finite at $r = 0$ and $r = \infty$. Furthermore, $\mu^{C,D}$ are the magnetic permeabilities of the respective media, $a_n^{C,D}$ and $b_n^{C,D}$ are constants determined from the boundary conditions,

$$K_j^2 = \omega^2 \epsilon_j(\omega)/c^2 - k_z^2 \quad \text{for} \quad j = C, D$$

and

$$S_n = \exp(in\theta + ik_z z - i\omega t) \,. \qquad (2.2)$$

By applying the boundary conditions, that the tangential components of the electric field $\vec{E}$ and the magnetic field $\vec{H}$ must be continuous at the cylinder surface, $r = a$, a system of four linear homogeneous equations is obtained which is satisfied by the four coefficients $a_n^{C,D}$ and $b_n^{C,D}$. This system of four homogeneous equations does not admit the simplified solutions with either all a's or all b's vanishing, corresponding to the magnetic and electric waves, respectively, except for the $n = 0$ mode (hence, the SP eigenmode is a superposition of both electric and magnetic waves).[11] The nontrivial solution is obtained by letting the determinant of the system vanish. The expansion of this determinant gives rise to the transcendental equation[11]

$$F(k_z, \omega) = \left(\frac{\mu_C}{K_C a} \frac{J_n'(K_C a)}{J_n(K_C a)} - \frac{\mu_D}{K_D a} \frac{H_n^{(1)\prime}(K_D a)}{H_n^{(1)}(K_D a)}\right)\left(\frac{(\omega/c)^2 \epsilon_C(\omega)}{\mu_C K_C a} \frac{J_n'(K_C a)}{J_n(K_C a)} - \frac{(\omega/c)^2 \epsilon_D(\omega)}{\mu_D K_D a} \frac{H_n^{(1)\prime}(K_D a)}{H_n^{(1)}(K_D a)}\right)$$

$$-n^2k_z^2\left(\frac{1}{(K_Da)^2}-\frac{1}{(K_Ca)^2}\right)^2 = 0 , \tag{2.3}$$

whose solutions are the dispersion relations, $\omega_n = \omega_n(k_z)$, of the natural modes of the system, the SP modes, for the propagation constant k_z and mode number n.

The θ dependence of the components of the electromagnetic field for the nth mode, Eq. (2.1), enters only through the factor $e^{in\theta}$ of Eq. (2.2). For the symmetrical mode, $n=0$, the fields are independent of θ. The coefficients, $a_0^{C,D}$ and $b_0^{C,D}$ are then independent of each other, and pure electric ($H_z=0$) and pure magnetic ($E_z=0$) waves are allowed solutions of Maxwell's equations in the circularly cylindrical geometry.[11] The pure electric wave, which gives rise to surface charge, leads to the trivial transcendental equation for $n=0$[11]

$$F(k_z,\omega)=\frac{(\omega/c)^2\epsilon_C(\omega)}{\mu_C K_C a}\frac{J_1(K_Ca)}{J_0(K_Ca)} - \frac{(\omega/c)^2\epsilon_D(\omega)}{\mu_D K_D a}\frac{H_1^{(1)}(K_Da)}{H_0^{(1)}(K_Da)} = 0 . \tag{2.4}$$

The SP mode, resulting from the solution of (2.4), has an uninteresting behavior compared to the SPO, with angular dependence ($n \geq 1$) whose fields are superpositions of electric and magnetic waves. There is only the real nonradiative branch to the surface mode; the corresponding $n=0$ virtual radiative mode does not exist. Moreover, this nonradiative branch lacks the minimum in its dispersion relation, a characteristic found in the $n \geq 1$ modes for certain curvature.

Since the fields of the $n=0$ mode are independent of θ, this SPO "sees" no curvature to the cylinder. The only variation in the fields is the periodic one along the cylinder axis, z, given by the factor e^{ik_zz} in (2.1) and (2.2). The surface charge forms periodic bands of opposite charge along the z direction. This is analogous to the bands of surface charge set up on a semi-infinite metallic plane by its real nonradiative mode.[3,5] Thus the $n=0$ cylindrical surface mode behaves similarly to the planar mode, having only a nonradiative branch with no minimum in its dispersion curve. The nonexistence of the virtual radiative $n=0$ mode has been verified by the authors in the numerical analysis of Sec. III with the substitution of (2.4) into Eq. (3.8). The real nonradiative $n=0$ mode has been studied by Englman and Ruppin[7] and Ashley and Emerson.[10]

III. NUMERICAL TECHNIQUES AND RESULTS

Before the equation $F(k_z,\omega)=0$ can be solved, it is necessary to know the form of the dielectric functions $\epsilon_C(\omega)$ and $\epsilon_D(\omega)$. The usual procedure is either to find the constitutive equations which relate the currents and charges in the specific system in terms of the electromagnetic fields, a step which often involves the development of sophisticated approximations, or to draw upon already developed approximations, choosing the one which best fits the specific system. A reasonable choice for the dielectric function of a metal[5] is the simple expression

$$\epsilon(\omega)=1-\omega_p^2/\omega^2 , \tag{3.1}$$

where ω_p is the bulk plasma frequency. The dielectric is assumed to be air with $\epsilon_D(\omega)=1$. Also, the media are assumed nonmagnetic so that $\mu_C \equiv 1$ and $\mu_D \equiv 1$.

By introducing the changes of variable

$$\Omega=\omega/\omega_p, \quad K=k_z/k_p=k_zc/\omega_p , \tag{3.2}$$

where Ω and K are now dimensionless variables, and the above results for $\epsilon_C(\omega)$, $\epsilon_D(\omega)$, and $\mu_{C,D}$, the arguments of the Bessel and Hankel functions become, respectively,

$$V_1=\alpha(\Omega^2-K^2-1)^{1/2} ,$$
$$V_2=\alpha(\Omega^2-K^2)^{1/2} \quad \text{with} \quad \alpha=k_pa=\omega_pa/c , \tag{3.3}$$

where a is the cylinder radius. Then, by rearranging the terms, the transcendental equation $F(k_z,\omega)=0$ is brought into a more simplified form,

$$F(K,\Omega)=(\Omega^2-1)(\Omega^2-K^2)^2X^2+\Omega^2(\Omega^2-K^2-1)^2Y^2 - (2\Omega^2-1)(\Omega^2-K^2)(\Omega^2-K^2-1)XY-n^2K^2=0 , \tag{3.4}$$

where n is the order or mode number,

$$X=V_1\frac{J_n'(V_1)}{J_n(V_1)}, \quad Y=V_2\frac{H_n^{(1)\prime}(V_2)}{H_n^{(1)}(V_2)} . \tag{3.5}$$

Before the start of the numerical investigation, the results of which are presented in Figs. 1–3, an analytical investigation, which is contained in the Appendix, was attempted. Certain general properties of the SPO were revealed,[7] which were later verified by the computer analysis. In brief, two distinct behaviors were found: (i) the SPO in the region of $K>\Omega$ are real nonradiative modes, real because the equation $F(K,\Omega)=0$ gives rise to real eigenfrequencies, $\Omega=\Omega(K)$, for real K, and

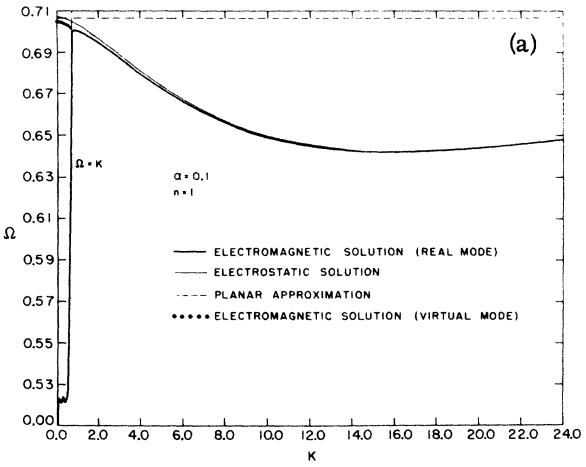

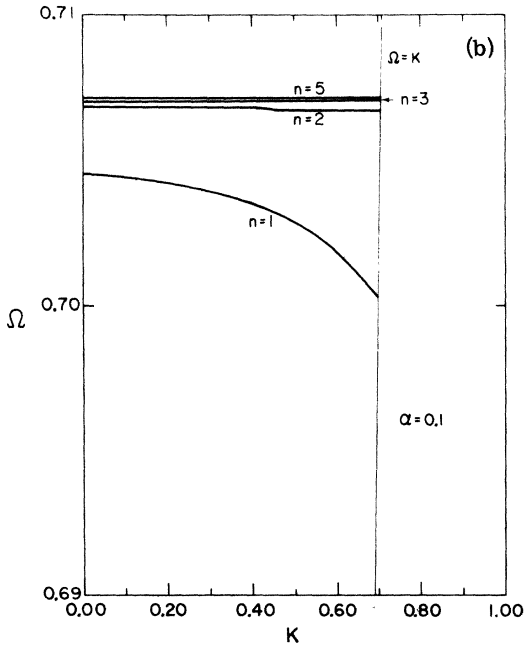

FIG. 1. (a) Dispersion relation for the $n=1$ SPO of a circular cylinder with $\alpha = k_p a = 0.1$, where $k_p = \omega_p/c$ is the plasma wave vector and a is the cylinder radius. $\Omega = \omega/\omega_p$ is the frequency normalized to the plasma frequency ω_p and $K = k_z/k_p$ is the normalized wave vector along the z axis, the cylinder axis. The electromagnetic solution is exact. The electrostatic and planar approximations (see text) are shown. (b) Dispersion relations for the $n=1$, 2, 3, and 5 virtual rediative SPO of a circular cylinder with $\alpha = k_p a = 0.1$, where $k_p = \omega_p/c$ is the plasma wave vector and a is the cylinder radius. $\Omega = \omega/\omega_p$ is the frequency ω_p and $K = k_z/k_p$ is the normalized wave vector along the z axis, the cylinder axis. The radiative modes are the exact electromagnetic solutions.

nonradiative because the electromagnetic fields associated with these modes decay exponentially to zero outside the cylinder; (ii) the SPO in the region of $K < \Omega$ are virtual radiative modes, virtual because $F(K, \Omega) = 0$ results in complex eigenfrequencies, $\Omega = \Omega(K)$, for real K, where the imaginary part of Ω is the inverse of the lifetime of each mode, which is now finite rather than infinite as for the case of the real modes, and radiative because the fields behave as propagating cylindrical waves for increasing r. The photon line, $K = \Omega$, is the line of demarcation for the SPO, such that the dispersion relations for the real modes can approach it asymptotically but never cross it.

The core of the numerical analysis was the subroutine which calculated the values of the Bessel functions. The standard computational techniques[13] were employed to calculate the Bessel, Neumann, and modified Bessel functions, $J_n(x)$, $Y_n(x)$, $I_n(x)$, and $K_n(x)$, for integer mode number n, and real argument x; the values were accurate through the fifth decimal place when compared with Watson's tables.[12]

The real modes were obtained initially.[5,10] An iteration procedure was used and thus required that Eq. (3.4) be rearranged so that the process converged,

$$\Omega = [n^2K^2 + (\Omega^2 - K^2)XQ]^{1/2}/Q ,$$

where

$$Q = (\Omega^2 - K^2)X - (\Omega^2 - K^2 - 1)Y , \tag{3.6}$$

and X and Y are defined by (3.5) and (3.3). The initial value of the iteration process is provided by the electrostatic limit[5,9] ($c \to \infty$) of (3.4), which simplifies to

$$\Omega = \left(\frac{X}{X - Y}\right)^{1/2} , \tag{3.7a}$$

where

$$X = V\frac{J_n'(V)}{J_n(V)} , \quad Y = V\frac{H_n^{(1)\prime}(V)}{H_n^{(1)}(V)} , \quad V = i\alpha K \tag{3.7b}$$

for the electric wave mode number n.

Because the argument V is imaginary, X and Y are real ratios (see the Appendix) and (3.7a) is a real exact relation for real K. This relation, called the electrostatic approximation, has the asymptotic behavior $-\Omega_{K\to\infty} 1/\sqrt{2}$ and $\Omega_{K\to 0} 1/\sqrt{2}$. It is a valid approximation[5,9] in the region of large K, i.e., $k_z \gg \omega/c$, for the eigenmodes of (3.4).

For the initial values of K, $K \gg 1$, (3.7) calculates the electrostatic value Ω_0, which is then inserted into (3.6) to calculate a new value Ω_1. Ω_1 is returned to (3.6) and the process continues until a certain accuracy is achieved, i.e., the value Ω_L after L iterations is within a certain error compared to the previous value, Ω_{L-1}; in the program, the same accuracy as that of the Bessel function values was desired, i.e., $|\Omega_L - \Omega_{L-1}|$

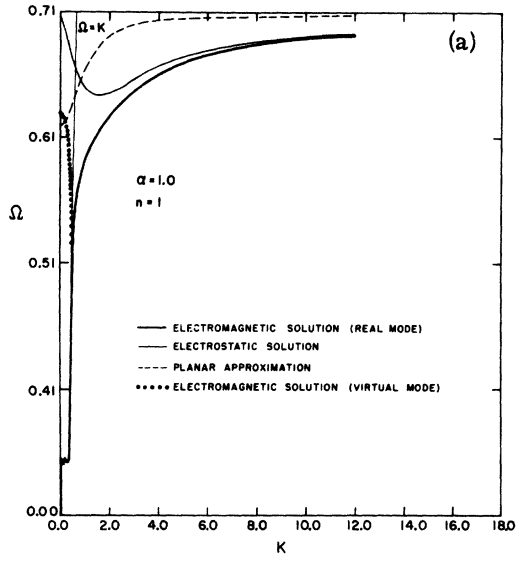

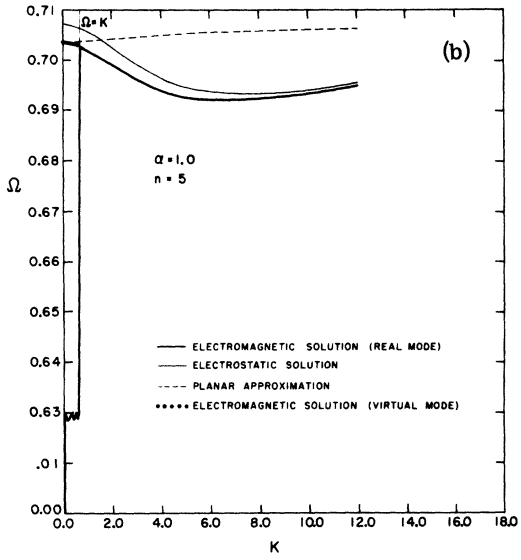

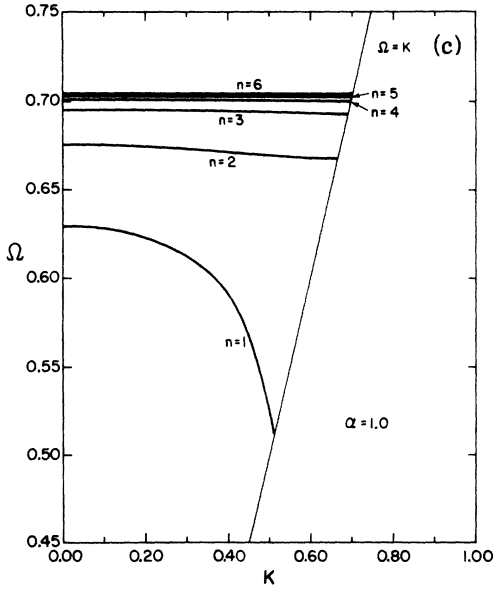

FIG. 2. (a) Dispersion relation for the $n=1$ SPO of a circular cylinder with $\alpha=k_p a=1.0$, where $k_p=\omega_p/c$ is the plasma wave vector and a is the cylinder radius. $\Omega=\omega/\omega_p$ is the frequency normalized to the plasma frequency ω_p and $K=k_z/k_p$ is the normalized wave vector along the z axis, the cylinder axis. The electromagnetic solution is exact. The electrostatic and planar approximations (see text) are shown. (b) Dispersion relation for the $n=5$ SPO of a circular cylinder with $\alpha=k_p a=1.0$, where $k_p=\omega_p/c$ is the plasma wave vector and a is the cylinder radius. $\Omega=\omega/\omega_p$ is the frequency normalized to the plasma frequency ω_p and $K=k_z/k_p$ is the normalized wave vector along the z axis, the cylinder axis. The electromagnetic solution is exact. The electrostatic and planar approximations (see text) are shown. (c) Dispersion relations for the $n=1,2,\ldots,6$ virtual radiative SPO of a circular cylinder with $\alpha=k_p a=1.0$, where $k_p=\omega_p/c$ is the plasma wave vector and a is the cylinder radius. $\Omega=\omega/\omega_p$ is the frequency normalized to the plasma frequency ω_p and $K=k_z/k_p$ is the normalized wave vector along the z axis, the cylinder axis. The radiative modes are the exact electromagnetic solutions.

$<10^{-5}$. Subsequently, for each succeeding value of K, instead of the electrostatic value at this K, the electromagnetic value at the previous point K is used in (3.6) for the iteration process (this was necessary because of the eventual inadequacy of the electrostatic approximation due to retardation effects). In this manner, the dispersion relations, $\Omega=\Omega(K)$, were obtained for the real modes.

However, this method was not applicable to the virtual modes, whose eigenfrequencies are complex, since the Bessel function subroutine requires that the arguments of the functions be real. Yet $|F(K,\Omega)|$ has a minimum at the point (K,Ω) for real K and Ω, $\Omega>K$, when Ω coincides with the real part of the complex eigenfrequency of a virtual mode. These modes appear as peaks in the function

$$G(K,\Omega)=\left|(\Omega^2-K^2)(\Omega^2-K^2-1)\right|/\left|F(K,\Omega)\right|, \tag{3.8}$$

where $F(K,\Omega)$ is given by (3.4) and where the numerator removes the background due to the trivial solutions, $\Omega^2=K^2$ and $\Omega^2=K^2+1$, of the equation $F(K,\Omega)=0$ (these solutions would otherwise obscure the virtual modes). The program thus calculated the values of $G(K,\Omega)$ at each point of a grid in the region of $\Omega>K$; the grid was made fine enough so that the real part of the complex eigenfrequency of each mode, the center point of the peak, and the imaginary part, the half-width of the

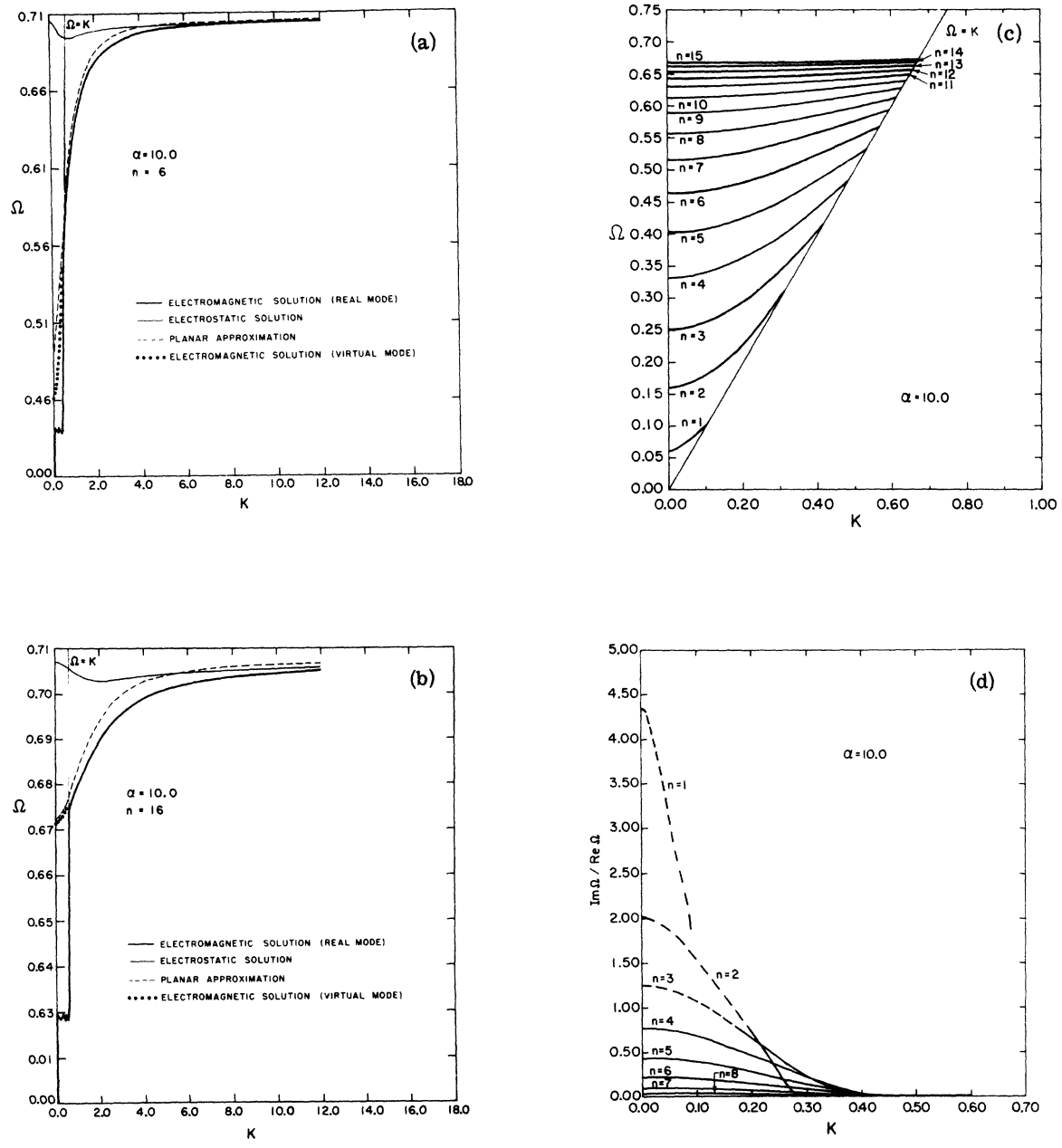

FIG. 3(a) Dispersion relation for the $n=6$ SPO of a circular cylinder with $\alpha = k_p a = 10.0$, where $k_p = \omega_p/c$ is the plasma wave vector and a is the cylinder radius. $\Omega = \omega/\omega_p$ is the frequency normalized to the plasma frequency ω_p and $K = k_z/k_p$ is the normalized wave vector along the z axis, the cylinder axis. The electromagnetic solution is exact. The electrostatic and planar approximations (see text) are shown. (b) Dispersion relation for the $n=16$ SPO of a circular cylinder with $\alpha = k_p a = 10.0$, where $k_p = \omega_p/c$ is the plasma wave vector and a is the cylinder radius. $\Omega = \omega/\omega_p$ is the frequency normalized to the plasma frequency ω_p and $K = k_z/k_p$ is the normalized wave vector along the z axis, the cylinder axis. The electromagnetic solution is exact. The electrostatic and planar approximations (see text) are shown. (c) Dispersion relations for the $n = 1, 2, \ldots, 15$ virtual radiative SPO of a circular cylinder with $\alpha = k_p a = 10.0$, where $k_p = \omega_p/c$ is the plasma wave vector and a is the cylinder radius. $\Omega = \omega/\omega_p$ is the frequency normalized to the plasma frequency ω_p and $K = k_z/k_p$ is the normalized wave vector along the z axis, the cylinder axis. The radiative modesare the exact electromagnetic solutions. (d) Graph of the ratio Im Ω/Re Ω vs the wave vector K for the $n = 1, 2, \ldots, 8$ virtual radiative SPO of a circular cylinder with $\alpha = k_p a = 10.0$, where $k_p = \omega_p/c$ is the plasma wave vector and a is the cylinder radius. $\Omega = \omega/\omega_p$ is the frequency normalized to the plasma frequency ω_p and $K = k_z/k_p$ is the normalized wave vector along the z axis, the cylinder axis. For Im $\Omega >$ Re Ω (dashed lines), the lifetimes are too short for the modes to be well defined; for Im $\Omega <$ Re Ω (solid lines), the modes become better defined. The curves terminate at the photon line.

peak, were accurate through the third decimal place.

The numerical analyses discussed previously were exact calculations of the SPO in a circularly cylindrical conductor. In addition, an approximation was employed, a technique devised by C. Miziumski[8] to explain his experimental results, which, for us, would serve only as a comparison for the actual modes. This approximate technique treated the cylinder as locally flat so that its SP eigenfunction is the same as for a semi-infinite plane; the curvature introduces only periodic boundary conditions. This approximation, henceforth referred to as the planar approximation, has some validity for very thick cylinders.[10]

The dispersion relation, for the SPO in a semi-infinite conductor, characterized by the dielectric function $\epsilon_C(\omega) = 1 - \omega_p^2/\omega^2$, in contact with a semi-infinite dielectric with $\epsilon_D(\omega) = 1$, is given by[5]

$$\omega = \omega_p[1 + \tfrac{1}{2}q^{-2} + (1 + \tfrac{1}{4}q^{-4})^{1/2}]^{-1/2}, \qquad q = k_\parallel/k_p , \tag{3.9}$$

where $k_\parallel$ is the wave vector parallel to the surface of the plane. The resulting SPO are real non-radiative modes with the asymptotic behavior, $\omega \xrightarrow[k_\parallel \to 0]{} ck_\parallel \to 0$ and $\omega \xrightarrow[k_\parallel \to \infty]{} \omega_p/\sqrt{2}$, where $k_\parallel > \omega/c$.

When (3.9) is applied to a locally flat cylinder, the properties of the cylinder enter through the wave vector, $k_\parallel$. We can then define

$$k_\parallel^2 = k_z^2 + k_\theta^2 , \tag{3.10}$$

where k_z and k_θ are the propagation constants in the z and θ directions, respectively. k_θ is inversely proportional to the wavelength λ_n^θ of the oscillation propagating along the cylinder's circumference; the cyclical boundary conditions determine this to be $\lambda_n^\theta = 2\pi a/n$, where n is the order of the oscillation and a the cylinder radius ($2\pi a$, the cylinder circumference), so that

$$k_\theta = 2\pi/\lambda_n^\theta = n/a . \tag{3.11}$$

Using (3.10 and 3.11), we get

$$q = k_\parallel/k_p = [(k_z/k_p)^2 + (n/\alpha)^2]^{1/2} , \tag{3.12}$$

where $\alpha = k_p a$ and the factor n/α determines the cylindricality of the system such that in a thick cylinder ($\alpha \gg 1$) n/α is a negligible factor for small n. Introducing (3.2) brings the dispersion relation (3.9) into the form

$$\Omega = [1 + \tfrac{1}{2}Q^{-2} + (1 + \tfrac{1}{4}Q^{-4})^{1/2}]^{-1/2}, \qquad Q = [K^2 + (n/\alpha)^2]^{1/2} , \tag{3.13}$$

so that the results, for mode number n and the parameter α, can be compared with the exact SPO. Equation (3.13) has the asymptotic behavior—$\Omega \xrightarrow[K \to \infty]{} 1/\sqrt{2}$ and at $K = 0$, $\Omega = \{1 + \tfrac{1}{2}(\alpha/n)^2 + [1 + \tfrac{1}{4}(\alpha/n)^4]^{1/2}\}^{-1/2}$, i.e., the photon line is crossed.

Some of the results of the computer analysis of SPO in a circularly cylindrical conductor are contained in Figs. 1–3. The graphs therein are separated into two types—those containing the dispersion relations, computed by the electrostatic and the planar approximations, and the exact electromagnetic equation for the virtual and real modes, for a certain n and α. Also shown are those containing the dispersion relations of the virtual radiative modes alone for the three values of α, where $\alpha = k_p a$ is a measure of the cylindricality of the system. The data were obtained for three values of α, 0.1, 1.0, and 10.0, i.e., the cylinders ranged from thin to thick (by varying only the radius a) or from fair to very good conductors (by varying only the plasma frequency ω_p where $k_p = \omega_p/c$).

Figure 1 contains the modes for $\alpha = 0.1$ and the results are applicable to systems with high cylindricality, i.e., $\alpha \ll 1$ or $n/\alpha \gg 1$. For all values of n, the mode number, the electrostatic approximation is an accurate approximation to the exact dispersion relations for the real modes. Of course for $K \leq 1.0$, retardation effects become noticeable as the electromagnetic curve bends and approaches the photon line asymptotically (with a difference of less than 10^{-5} for $K \leq 0.6$) while the electrostatic curve continues across. As was expected, the planar approximation is invalid for systems with high cylindricality, exhibiting constant behavior $\Omega \approx 1/\sqrt{2}$, for $0 < K < \infty$.

A very interesting feature of the real modes is the minimum in the dispersion curve, e.g., Fig. 1(a), for the $n = 1$ mode. The position and value of the minimum depends on n such that for $n = 1$ the frequency is 9.2% less than $1/\sqrt{2}$ and the minimum appears at $K = 15.7$. As n increases, it shifts to higher K, according to the relation $K_{\min} \approx 1.5\, n/\alpha$, and the frequency rises: for $n = 2$, $K_{\min} = 29.5$ and $\Delta\Omega = 4.8\%$, and for $n = 3$, $K_{\min} = 43.3$ and $\Delta\Omega = 3.2\%$.

In order to understand the occurrence of the minimum we can first use electrostatic considerations and then examine what modifications retardation effects bring. Electrostatically both at $k_z = 0$ and $k_z = \infty$ the curvature of the cylindrical surface does not influence the eigenfrequency which remains as in the plane case: $\omega_p/\sqrt{2}$. At $k_z = \infty$ the above statement is obvious since this $k_z = \infty$ wave sees the surface as flat, at $k_z = 0$ one can calculate the eigenfrequency as the pole in the attraction force between the cylinder under consideration and a parallel straight wire carrying a uniform oscillating (in time) charge $q(t) = q_0 e^{i\omega t}$. This force is proportional to the image charge $q'(t)$ and the latter is the same as in the plane geometry, name-

ly $q'(t)=[1-\epsilon(\omega)]q(t)/[1+\epsilon(\omega)]$. Hence, in both cases the SP eigenfrequency is given (electrostatically) by the solution of the equation $1+\epsilon(\omega)=0$. Thus we need a variation of the fields along the axis direction in order to make the effects of the curvature of the cylindrical surface felt. On the basis of the previous arguments we expect that these effects will be more significant when $k_z \approx k_\theta = n/\alpha$. By comparing with the results for a sphere {where the eigenfrequency $\omega_l=\omega_p/[1+(1+1/l)]^{1/2} < \omega_p/\sqrt{2}$} one expects that the effects of the curvature of the cylindrical surface would be to decrease the eigenfrequency, and consequently to create a minimum when $k_z \approx n/a$, in agreement with our results. One also expects that as n increases, for a given α, the effects of the curvature would be less and less pronounced; this property is in agreement with our results too.

When the minimum occurs well to the right of the c line, the above electrostatic picture for the minimum is valid [see Figs. 1(a) and 2(b)]. When the minimum is close to or to the left of the c line, retardation effects invalidate the electrostatic description and the minimum actually disappears [see Figs. 2(a), 3(a), and 3(b)].

For $\alpha=0.1$ the virtual modes are well-defined radiative modes with the half-width $\mathrm{Im}\Omega \leq 0.01 \times \mathrm{Re}\Omega$ for all n and for all values of K from $K=0.0$ to the photon line and with $\mathrm{Re}\Omega \approx 1/\sqrt{2}$. Despite the constancy in frequency, $\mathrm{Re}\Omega$, which Fig. 1(b) shows, there is some variation according to n and K for the virtual modes, a behavior which becomes more noticeable for higher α. For example, the $n=1$ mode has $\mathrm{Re}\Omega=0.7044$ and $\mathrm{Im}\Omega=0.0046$ at $K=0.0$, values which change to $\mathrm{Re}\Omega=0.7019$ and $\mathrm{Im}\Omega=0.0083$ at $K=0.06$. The modes for $n \geq 2$ show negligible change in half-width with $\mathrm{Im}\Omega < 0.0001$.

Figure 2 contains the modes for $\alpha=1.0$ and the results are applicable to systems with moderate cylindricality, i.e., $\alpha \approx 1.0$ or $0.5 < n/\alpha < 5$. For the lower modes, $n \leq 4$, the electrostatic approximation is no longer as accurate an approximation to the exact dispersion relations as in a highly cylindrical system; for $n \geq 5$ the system can be considered highly cylindrical. Moreover, the planar curves show more variation with respect to K: this variation is greatest for $n=1$ and decreases for increasing n until the constancy of frequency ($\approx 1/\sqrt{2}$) of highly cylindrical systems is recaptured for $n \geq 5$.

The minima in the dispersion curves have been affected by the increase in α. The minimum in the $n=1$ mode has disappeared entirely while for $n \geq 2$ the locations of the minima are still proportional to the factor n/α, i.e., $K_{\min} \approx 1.3\, n/\alpha$ for $n \geq 2$, a marked shift towards the photon line. The frequencies differ from $1/\sqrt{2}$ by the amounts 6.1% at $K_{\min}=2.1$ for $n=2$, 3.7% at $K_{\min}=3.7$ for $n=3$, 2.7% at $K_{\min}=5.1$ for $n=4$, and 2.1% at $K_{\min}=6.5$ for $n=5$. Figures 2(a) and 2(b) give the dispersion curves for $n=1$ and $n=5$, respectively.

The virtual radiative modes have been altered by the change from high to moderate cylindricality. The $n=1$ mode has peeled off from the group of modes with frequency $\approx 1/\sqrt{2}$ and lies at $\Omega \approx 0.6$. Moreover, it is poorly defined with $\mathrm{Im}\Omega=0.602 \times \mathrm{Re}\Omega$ at $K=0.0$, which increases to $\mathrm{Im}\Omega=1.331 \times \mathrm{Re}\Omega$ at $K=0.5$. The $n=2$ mode is better defined with $\mathrm{Re}\Omega=0.6756$ and $\mathrm{Im}\Omega=0.0223$ at $K=0.0$, values which change to $\mathrm{Re}\Omega=0.6679$ and $\mathrm{Im}\Omega=0.0075$ at $K=0.06$. The $n \geq 3$ modes recapture the well-defined character of the modes of the highly cylindrical system with $\mathrm{Im}\Omega \leq 0.0001$ for the K range of $K=0.0$ to the photon line. These modes, $1 \leq n \leq 6$, are contained in Fig. 2(c).

A third system was examined, that with $\alpha=10.0$. The results are applicable to systems with low cylindricality, i.e., $\alpha \gg 1.0$ or $n/\alpha \ll 1.0$. The real nonradiative modes for $n=6$ and 16, are contained in Figs. 3(a) and 3(b), while the virtual radiative modes, $1 \leq n \leq 15$, are in Fig. 3(c). The variation of the inverse lifetimes of the lower-lying modes, $n \leq 8$, with respect to the wave vector K, is shown in Fig. 3(d) where $\mathrm{Im}\Omega/\mathrm{Re}\Omega$ is plotted against K.

A change has occurred in the real modes; the minima no longer exist. They are still present in the electrostatic approximations for the modes observed, i.e., for $1 \leq n \leq 20$, but not in the electromagnetic curves. Instead, the dispersion curves decrease gradually from $\Omega \approx 1/\sqrt{2}$ for $K \gg 1$ until $K < 5.0$ when the retardation effects bend the curves toward the photon line. The electrostatic approximations diverge from the exact solutions in this region. Yet, the planar curves do not, verifying thus the assumption that the planar approximation should be valid for $\alpha \gg 1.0$.

The virtual modes also show interesting behavior. They are now spread across the region delineated by $\Omega=1/\sqrt{2}$, $K=0.0$, and the photon line. The lower modes have lifetimes so short that they are almost nonexistent except near the photon line where they become better defined. For example, the $n=1$ mode has $\mathrm{Re}\Omega < 0.1$ and $\mathrm{Im}\Omega \geq 2.0\,\mathrm{Re}\Omega$, the $n=2$ mode is better defined with $\mathrm{Re}\Omega=0.1586$ and $\mathrm{Im}\Omega=0.319$ at $K=0.0$, values which change to $\mathrm{Re}\Omega=0.3006$ and $\mathrm{Im}\Omega=0.002$ at $K=0.3$, and the $n=3$ mode has $\mathrm{Re}\Omega=0.2491$ and $\mathrm{Im}\Omega=0.312$ at $K=0.0$ and $\mathrm{Re}\Omega=0.4043$ and $\mathrm{Im}\Omega=0.002$ at $K=0.4$. The intermediate modes, $4 \leq n \leq 8$, show similar variation with respect to K but with progressively longer lifetimes. The modes for $n \geq 9$ are well defined with $\mathrm{Im}\Omega \leq 0.01\,\mathrm{Re}\Omega$. Moreover, the real part of the eigenfrequency for these modes remains fairly constant in the range $0.0 \leq K <$ photon line,

whereas for $n \leq 8$, $\Delta \mathrm{Re}\Omega > 0.04$, an appreciable increase in $\mathrm{Re}\Omega$ with respect to K.

The planar approximation can in certain limiting cases be used to estimate the real parts of the complex eigenfrequencies, $\mathrm{Re}\Omega$, of the radiative modes (Figs. 1–3 illustrate the varying accuracy of the approximation). However, this is the only information that can be obtained from this approximation. The electromagnetic solution of Eq. (3.4) gives also the decay rate ($\equiv \mathrm{Im}\Omega$),[5] the dependence on mode number n and wave vector K automatically.

Before we conclude this section we would like to draw attention to the quite different behavior of the $\mathrm{Re}\Omega$ and $\mathrm{Im}\Omega$ as a function of k_z for the modes $n=1$, $\alpha=0.1$, $\alpha=1.0$ [Figs. 1(b) and 2(c)] on one hand, and the modes $n=4$, 5, etc., $\alpha=10$ on the other hand. One can understand this difference on the basis of results for the plane geometry. The former modes ($n=1$, $\alpha=0.1$, $\alpha=1$) are somehow similar with the radiative plasmons in thin films in the sense that both are due to surface charges of opposite sign situated opposite to each other. The behavior of $\mathrm{Re}\Omega$ and $\mathrm{Im}\Omega$ is similar to the thin-film virtual mode; i.e., $\mathrm{Re}\Omega$ decreases with k_z while $\mathrm{Im}\Omega$ increases with k_z. On the other hand, the modes for $\alpha=10$ ($n=4$, 5, etc.) are similar to thick-film modes in the sense that opposite surface charges sit next to each other (due to the large values of α the charges located diametrically are almost decoupled). This observation together with the known results for a single surface explains the behavior of these modes as a function of k_z, namely the increase of $\mathrm{Re}\Omega$ and decrease of $\mathrm{Im}\Omega$ with increasing k_z. Of course modes with in-between behavior are present, e.g., the modes $\alpha=1$, $n=2$, 3, etc.

IV. COMPARISON WITH EXISTING EXPERIMENT

One method of experimental detection of SPO involves the scattering of light from the electron gas confined to a smooth metallic surface. If the scattering is inelastic such as by the coupling of the photons to the elementary excitations of the system, i.e., surface plasmons, structure is introduced in the optical properties of the system. The position of this structure, i.e., peaks or dips in the reflectance and transmission of the light, is determined from the resonance condition, i.e., the matching of the frequencies and the wave vectors of the photons and the SP. The details of the structure (the linewidth, strength, shape, etc. of the peaks and dips) usually require a quantitative investigation of the photon-SP interaction. However, extensive experimentation on the interaction of light with metallic surfaces of various geometries, e.g., the plane, thin and thick films, and the sphere, has verified the above qualitative statements and have shown them to be geometry independent (Refs. 3 and 5 provide reviews of the relevant material).

Consequently, as we shall discuss below, structure in the optical properties of metallic cylinders was found at the position expected from the resonance condition for photon-SP interaction. This fact together with the extensive experimentation in the other geometries leads to the conclusion that the observed structure is indeed due to the SP excitation by light. A further confirmation of this would demand a quantitative study of the interaction, a project which is currently under investigation.

Miziumski[8] performed an optical experiment to detect the SPO in a cylinder. It consisted of illuminating a metallic cylinder with a laser. The intensity of reflected light was then measured by a photocell as a function of β, the angle of incidence with respect to the cylinder axis. The reflected intensity of the laser light, as β was varied, showed regularly spaced dips, a structure explained by the excitation of SPO. This structure occurred for $1^\circ \leq \beta \leq 5^\circ$ and was associated with the modes, $55 \leq n \leq 58$, as computed from[8]

$$\omega \cos\beta_n(\omega) = c k_z(\omega) , \tag{4.1}$$

where $k_z(\omega)$ is obtained from the planar approximation, Eqs. (3.9) and (3.11), as a function of ω and n.

Aluminum was evaporated onto a quartz fiber with a radius of 25 μm, forming a cylinder of radius $a=29$ μm, with a bulk plasma wavelength $\lambda_p = 828$ Å, for this optical experiment. It was then illuminated by an He-Ne laser of wavelength $\lambda = 6328$ Å. These values can be converted to the system of parameters given by (3.2):

$$\begin{aligned} &\alpha = k_p a = 2200, \\ &\Omega_L = \omega/\omega_p = 0.131 , \\ &K = k_z/k_p = \Omega_L \cos\beta = 0.131 \cos\beta . \end{aligned} \tag{4.2}$$

The value of α shows that Miziumzki's system is one of extremely low cylindricality where the plannar approximation should give reasonably accurate estimates of the real parts of the eigenfrequencies of the radiative modes. As noted previously, however, the lifetime of these modes cannot be obtained from the planar approximation.

It is not possible to obtain the eigenfrequencies of the radiative SP numerically via Eqs. (3.3)–(3.5) for $\alpha=2200$ because the arguments of the Bessel functions are too large.[13] Instead, extrapolation of the results for $\alpha=10.0$, as shown in Figs. 3(c) and 3(d), permits us to discuss the behavior of the virtual radiative modes for this system. First of all, we should expect that the region, delineated by $K=0.0$, $\Omega=1/\sqrt{2}$, and the photon line, will be densely populated by the virtual

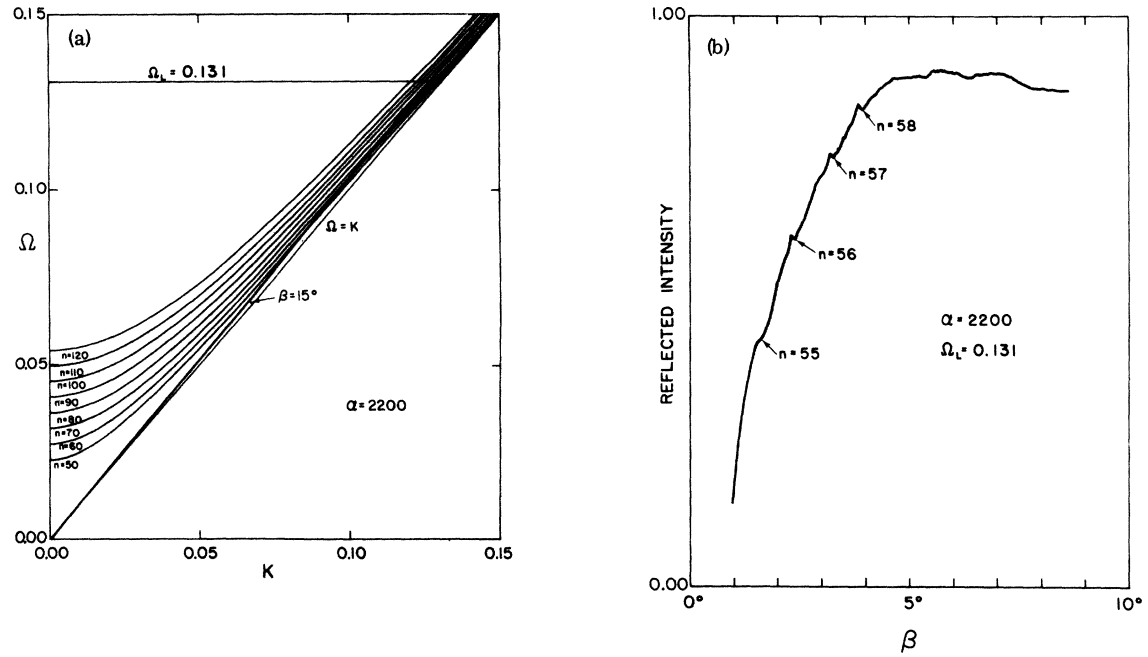

FIG. 4. (a) Dispersion relations for some of the SPO involved in Mizuinski's optical experiment, calculated according to the planar approximation (see text) which is almost exact for this case. An aluminum circular cylinder of radius 29 μ with a bulk plasma wavelength of 828 Å is illuminated by an He-Ne laser of wavelength 6328 Å. β is the angle of incidence of the laser light, $\Omega_L = \omega/\omega_p = 0.131$ is its frequency normalized to the bulk plasma frequency ω_p, $\alpha = k_p a = 2200$, where $k_p = \omega_p/c$ is the plasma wave vector and a is the cylinder radius, and $K = k_z/k_p$ is the normalized wave vector along the z axis, the cylinder axis. The frequency Ω_L and wave vector K are related by $K = \Omega_L \cos\beta$. The laser can excite SPO of the same Ω_L and K. (b) Reflected intensity of the laser vs the angle of incidence β reveals a sequence of dips corresponding to the excitation of the $n = 55$, 56, 57, and 58 SPO as calculated from the planar approximation [after Miziumski (Ref. 8)]. An He-Ne laser of wavelength 6328 Å illuminated an aluminum circular cylinder of radius $a = 29$ μ with a plasma wavelength 828 Å, such that $\Omega_L = \omega/\omega_p = 0.131$ is the laser frequency normalized to the plasma frequency ω_p of aluminum, $K = k_z/k_p$ is the normalized wave vector along the z axis, the cylinder axis, and $\alpha = k_p a = 2200$.

modes. Some of these modes are shown in Fig. 4(a). The lowest modes will have disappeared entirely, as almost with the $n = 1$ mode for $\alpha = 10.0$, thus creating a threshold number n_0, i.e., $n_0/\alpha \ll 1$, such that the modes, $n \geq n_0$, can be observed. Moreover, we should expect three regions where these radiative SPO will exhibit different properties, i.e., different degrees of definition, or progressively longer lifetimes.

These regions are: (i) $0.0 \leq \Omega < 0.3$, (ii) $0.3 \leq \Omega < 0.6$, and (iii) $0.6 \leq \Omega \leq 1/\sqrt{2}$. The first region contains modes with very short lifetimes, with $\mathrm{Im}\Omega \geq \mathrm{Re}\Omega$ at $K = 0.0$; the modes become better defined with increasing $\mathrm{Re}\Omega$ as the photon line is approached. The second region will contain the intermediate modes with progressively longer lifetimes, with $\mathrm{Re}\Omega > \mathrm{Im}\Omega > 0.01\ \mathrm{Re}\Omega$; these will be even more closely spaced but will not show as much variation with respect to K as the region (i) modes. These intermediate modes will, of course, become better defined as the photon line is approached, and correspond in behavior to the modes $4 \leq n \leq 9$ for $\alpha = 10.0$ in Fig. 3. The extremely well-defined modes with $\mathrm{Im}\Omega < 0.001$ are contained in the third region; these will be almost constant in frequency, $\mathrm{Re}\Omega$, and extremely closely spaced.

Miziumski's experiment occurred in region (i), in close proximity to the photon line, since $\Omega_L = 0.131$ and $K = \Omega_L \cos\beta \approx 0.131$ for $\beta < 5°$. Although the modes are better defined near the photon line, their lifetimes are still so short that little energy is absorbed by the system and the reflected intensity shows the weak structure depicted in Fig. 4(b). No further dips were observed after $\beta = 5°$ because, as β increases, K decreases, so that the lifetimes of the modes are decreasing, as expected. Also the dips are separated by only about 40 min of arc which verifies the expected density of the modes.

A threefold increase in Ω_L will push the experiment into the second region where the lifetimes of the radiative modes are much longer. The structure in the reflected intensity as a function of the incident angle β should now be enhanced. The dips are more pronounced; β is no longer limited to less than 5° either, because of the longer lifetimes

of the SP in general in this region. However, the structure should weaken as β increases because of the expected decreasing lifetime. Furthermore, a fivefold increase in Ω_L would push the experiment in region (iii). The modes should be very closely packed in this region; however, not so many can be excited by the incoming photon because of the constancy of their eigenfrequency. Thus, distinct dips, indicating excitation of the individual SPO, could be probably detected.

Ω_L can be increased with only minor modifications of the system. This is effected either by substituting a laser with a higher frequency, i.e., by increasing only ω which causes an increase in Ω_L with no change in α, or by using cylinders of different metals with lower plasma frequency, i.e., by decreasing ω_p which causes an increase in Ω_L as well as a decrease in α, or both.

It should be noted that repeating Miziumski's experiment with higher Ω_L and lower α (which can also be achieved by decreasing the diameter of the cylinder) would produce much more pronounced structure in the reflected intensity of the laser beam.

V. DISCUSSION

In this section we present a brief qualitative discussion about possible physical consequences of our results. A detailed quantitative study of the subject discussed here is presently under way.

We consider first the excitation of the real SP by any one of the well-known methods, i.e., interaction with external charged particles, mainly electrons of high (keV) or low (eV) energy or photons. For a thick enough cylinder ($\alpha \gg 1$) we expect line shapes and total cross sections similar to those encountered in flat surfaces. However, as α becomes smaller and smaller the minimum in the dispersion relation should appear and influence the line shape. For $\alpha \leq 1$ one expects the minimum to show in the line shape as a steeply rising precursor peak joining smoothly the lower side of the main broad peak at $\omega_p/\sqrt{2}$. Such a peculiar line shape, which is characteristic of SP in cylinders, requires for its observation a resolution of better than $\frac{1}{15}\omega_p$ and an α of one or less. The latter condition implies a radius of 500 Å or less for a typical metal and of 10^{-3} cm for a typical doped semiconductor. Note also that the existence of the minimum would have important consequences on whatever effects are due to plasmon-plasmon interactions, e.g., in experiments involving two-plasmon production.[14]

It is much more interesting to study experimentally the radiation associated with the virtual SP in cylinders. As we have seen, a variety of modes exists exhibiting different eigenfrequencies and quite different linewidths. What is more, the variation of the eigenfrequencies and linewidths with k_z (i.e., with the angle of emittance of the radiation) shows quite different behavior for different modes. Thus, a wealth of physical situations is present awaiting its experimental verification and study. Miziumski's experiment has shown clearly that the radiative SP are detectable even in quite thick cylinders. However, it is much more interesting to study the radiative SP in not so thick cylinders, because, then, the modes are better defined, well separated, and exhibit a variety of different behaviors. It would be very interesting to study the radiative SP in cylinders of α less than 100 to α of the order 1. For a typical metal this implies radii from 10^{-4} cm to 10^{-6} cm, respectively; for a doped semiconductor the corresponding numbers are 10^{-2}–10^{-4} cm. The experimental techniques used for the study of SP in plane surfaces and sphere can be used in the present geometry.

The results presented in this work allow a direct calculation of the radiation emitted during one period by one SP. Indeed this radiated energy equals $\hbar\,\mathrm{Im}\omega$. Thus all one has to do is to calculate the cross section for exciting SP by the external source in each particular case.

One case of possible importance is the excitation of SP by external electrons which stay close to the surface so as to maximize the electron-SP interaction. The cylindrical geometry allows the realization of such a configuration if one employs a static magnetic field parallel to the axis of the cylinder. Then the external electrons can revolve around the cylinder in circular orbits exciting continuously SP which in turn radiate. This process can be sustained at the expense of an externally supplied electronic kinetic energy. The frequency of the emitted radiation which falls in the ultraviolet for a metallic cylinder makes this possibility very attractive. To calculate the emitted radiation one has simply to find the cross section for exciting a SP by a revolving external electron and then calculate the steady-state distribution of SP due to their excitation by the external electrons as well as to the inverse process of absorption of existing SP by the electrons. The electron-SP cross section can be calculated by an extension of the methods used in plane and spherical geometries.[5]

It is useful to examine the problem of excitation of radiative SP in another way. An electron revolving in a circular orbit with a frequency ω_0 emits radiation which can be Fourier analyzed to components characterized by a wave vector $\tilde{k}_z$ (the z axis is perpendicular to the plane of the orbit) and a frequency $m\omega_0$ where m is a positive integer. Each such component acts as an external "force" on the cylinder under consideration.

Whenever the frequency $m\omega_0$ and wave vector $\tilde{k}_z$ coincide with an eigenfrequency $\omega_n(k_z)$ and eigenvector k_z of the natural modes of the system (i.e., the SP) a resonance condition is satisfied and a significantly enhanced radiation should be observed. The condition for this resonant enhancement of an harmonic $m\omega_0$ is

$$m\omega_0 = \omega_n(k_z) \ . \tag{5.1}$$

Whenever the eigenfrequency $\omega_n(k_z)$ is almost k_z independent the enhancement is expected to be very significant. Since ω_0 is proportional to the external static field we can satisfy Eq. (5.1) for various values of m. One can in principle see a successive enhancement of various harmonics $m\omega_0 (m = 1, 2, 3, \ldots)$ by decreasing the external field from a maximum value for which $\omega_0 = \omega_n(k_z)$. For a metallic cylinder even for the highest available fields Eq. (5.1) can be satisfied only for very high m (of the order of 100 or larger) where the spectrum is essentially a continuum one and the various harmonic cannot be resolved. On the other hand, for a doped semiconductor ω_0 can be almost of the same magnitude as ω_p and the enhancement of successive harmonics can be observed. Note, however, that, when $\omega_0 \sim \omega_p$, the original dielectric function $\epsilon(\omega) = 1 - \omega_p^2/\omega^2$ is modified[5] depending now not only on ω_p but on the new frequency ω_0. This would complicate and modify the results reported here but the method of theoretical study and the qualitative aspects discussed above will remain unchanged.

ACKNOWLEDGMENTS

We have benefitted from discussions with V. Celli and E. D. Palik. This work was partly supported by the National Science Foundation under Grant No. NSF-GH34404.

APPENDIX

In this section, it will be shown that, despite the fact that $F(k_z, \omega) = 0$ cannot be solved by analytical methods, the general behavior of the SPO in a circularly cylindrical conductor can be revealed.[7] The nature of the modes, whether radiative or nonradiative and real or virtual, will be determined. Moreover, the behavior of the dispersion relations in the vicinity of the photon line will be studied. This will be accomplished by using the properties of the Bessel and Hankel functions contained in G. N. Watson.[12]

The radiative or nonradiative character of the SPO is determined by whether the electromagnetic fields associated with the surface plasma have the form of traveling waves or exponentially decaying waves outside the cylinder, $r > a$. The field components are given by (2.1), (2.2), and the dielectric function $\epsilon_D(\omega) = 1$ so that the fields' behavior is dependent upon the behavior of the Hankel function $H_n^{(1)}(x)$ for order n and argument $x \equiv K_D r = r[(\omega/c)^2 \epsilon_D(\omega) - k_z^2]^{1/2} = r[(\omega/c)^2 - k_z^2]^{1/2}$. For $k_z > \omega/c$, x is imaginary, i.e., $x = ir(k_z^2 - \omega/c)^{1/2} \equiv ix^*$ where $x^* > 0$, and the Hankel function $H_n^{(1)}(ix^*)$ is related to the modified Bessel function $K_n(x^*)$ which decays exponentially for increasing r.[12] For $\omega/c > k_z$, x is real and $H_n^{(1)}(x)$ behaves as a traveling cylindrical wave for $r \gg a$.[12] Thus, for $k_z > \omega/c$ the SPO are nonradiative modes with exponentially decaying fields outside the cylinder, whereas for $\omega/c > k_z$ the SPO are radiative with fields acting like traveling cylindrical waves.

The real or virtual character of the SPO is determined by whether the solutions of $F(k_z, \omega) = 0$, $\omega_n = \omega_n(k_z)$ for real k_z, are either real or complex. A real mode has an infinite lifetime, i.e., the imaginary part of the eigenfrequency is zero, while a virtual mode has a finite lifetime, i.e., the imaginary part is nonzero. Yet we can state immediately that, since the SPO for $\omega/c > k_z$ are radiative, they must be virtual modes, otherwise conservation of energy would be violated. However, the nonradiative modes are not open to immediate prediction and their character can only be determined by further manipulation of the properties of $J_n(x)$ and $H_n^{(1)}(x)$.

The ratios X and Y, given by (3.3) and (3.5), are the important factors in $F(K, \Omega)$, i.e., Eq. (3.4). When $K > \Omega$, both arguments V_1 and V_2 are imaginary; i.e.,

$$\begin{aligned} V_1 &= i\alpha(K^2 + 1 - \Omega^2)^{1/2} = iV_1^* \ , \\ V_2 &= i\alpha(K^2 - \Omega^2)^{1/2} = iV_2^* \ , \end{aligned} \tag{A1}$$

so that X and Y are defined by the modified Bessel functions $I_n(V_1^*)$ and $K_n(V_2^*)$:

$$\begin{aligned} X &= iV_1^* \frac{J_n'(iV_1^*)}{J_n(iV_1^*)} = V_1^* \frac{I_n'(V_1^*)}{I_n(V_1^*)} \ , \\ Y &= iV_2^* \frac{H_n^{(1)\prime}(iV_2^*)}{H_n^{(1)}(iV_2^*)} = V_2^* \frac{K_n'(V_2^*)}{K_n(V_2^*)} \ , \end{aligned} \tag{A2}$$

where the prime now denotes differentiation with respect to V_1^* or V_2^*. Because $I_n(V_1^*)$ and $K_n(V_2^*)$ are real positive functions,[12] X and Y are now real positive ratios and $F(K, \Omega) = 0$ is thus a real equation. In similar manner, for $K < \Omega < (K^2 + 1)^{1/2}$, V_1 is imaginary and V_2 is real so that the ratios are

$$X = V_1^* \frac{I_n'(V_1^*)}{I_n(V_1^*)} \ , \quad Y = V_2 \frac{H_n^{(1)\prime}(V_2)}{H_n^{(1)}(V_2)} \ . \tag{A3}$$

X is real and positive as before, but Y is complex because the Hankel functions $H_n^{(1)}(V_2)$ are complex for all n. Thus, $F(K, \Omega) = 0$ is a complex equation and gives rise to the virtual radiative modes for $\Omega > K$. However, we suspect that the eigensolutions for $K > \Omega$ will be real because of the real

character of $F(K, \Omega)$ in this region.

The behavior of $F(K, \Omega)$ in the vicinity of the photon line is determined by the ratio Y. The vanishing of the argument V_2 causes the Hankel functions to blow up, thus allowing $H_n^{(1)}(V_2)$ to be evaluated through the infinite series,[12]

$$H_n^{(1)}(V_2) = J_n(V_2) + iY_n(V_2) = \left[1 + \frac{2i}{\pi}\left(\ln(\tfrac{1}{2}V_2) + \gamma - \frac{1}{2}\sum_{l=1}^{n}\frac{1}{l}\right)\right] J_n(V_2) - \frac{i}{\pi}\sum_{k=0}^{\infty}(-1)^k \frac{(\frac{1}{2}V_2)^{n+2k}}{k!\,(n+k)!}\sum_{l=1}^{k}\left(\frac{1}{l} + \frac{1}{n+l}\right)$$
$$- \frac{i}{\pi}\sum_{l=0}^{n-1}\frac{(n-l-1)!}{l!}(\tfrac{1}{2}V_2)^{-n+2l}, \qquad \text{(A4)}$$

where

$$J_n(V_2) = \sum_{l=0}^{\infty}\frac{(-1)^l}{l!\,(n+l)!}(\tfrac{1}{2}V_2)^{n+2l}$$

and $\gamma = 0.577215\ldots$, because of rapid convergence of the terms. Thus as $K \to \Omega$ we define $\delta \equiv (\Omega^2 - K^2)^{1/2} \ll 1$ so that by (3.3) we get

$$V_2 \equiv \alpha\delta, \quad V_1 \equiv \alpha(\delta^2 - 1)^{1/2} \to \alpha(-1)^{1/2} = i\alpha . \qquad \text{(A5)}$$

Moreover, because V_1 is imaginary and a constant, the ratio X is a real positive constant, i.e., by (A2)

$$X = \alpha[I_n'(\alpha)/I_n(\alpha)] . \qquad \text{(A6)}$$

Because of the similarity of behavior of the Hankel functions for all n at the origin, we expect a similarity of behavior of $F(K, \Omega)$ for all n in the vicinity of the photon line. Thus, $F(K, \Omega)$ for $n = 1$ will be examined. Moreover, only terms up to order δ^2 will be kept in the series expansion because of the factors $\ln(\frac{1}{2}V_2)$ and

$$\sum_{l=0}^{n-1}\frac{(n-l-1)!}{l!}(\tfrac{1}{2}V_2)^{-n+2l}$$

dominate the expansion.

The recurrence relations[12]

$$\tfrac{1}{2}[I_{n-1}(x) + I_{n+1}(x)] = I_n'(x) ,$$
$$\tfrac{1}{2}[H_{n-1}^{(1)}(x) - H_{n+1}^{(1)}(x)] = H_n^{(1)\prime}(x) , \qquad \text{(A7)}$$

are now used to obtain X and Y for $n = 1$, such that

$$X = \tfrac{1}{2}\alpha\,\frac{I_0(\alpha) + I_2(\alpha)}{I_1(\alpha)} ,$$
$$Y = \alpha\delta\,\frac{H_0^{(1)}(\alpha\delta) - H_2^{(1)}(\alpha\delta)}{H_1^{(1)}(\alpha\delta)} \qquad \text{(A8)}$$

by (A3), (A5), and (A6). The series expansion (A4) up to order δ^2 gives

$$H_0^{(1)}(\alpha\delta) = \{1 + (i/\pi)[2\gamma + 2\ln(\tfrac{1}{2}\alpha\delta) - 1]\} - (\tfrac{1}{2}\alpha\delta)^2[1 + (2i/\pi)(\gamma - 1)] ,$$
$$H_1^{(1)}(\alpha\delta) = \{1 + (2i/\pi)[\ln(\tfrac{1}{2}\alpha\delta) + \gamma - 1]\}(\tfrac{1}{2}\alpha\delta) - (i/\pi)(\tfrac{1}{2}\alpha\delta)^{-1} , \qquad \text{(A9)}$$
$$H_2^{(1)}(\alpha\delta) = [1 + (i/\pi)(2\gamma - \tfrac{5}{2})]\,\tfrac{1}{2}(\tfrac{1}{2}\alpha\delta)^2 - (i/\pi)[1 + (\tfrac{1}{2}\alpha\delta)^{-2}] .$$

Inserting (A9) into (A8) gives

$$Y = \frac{1 + [2\gamma + 2\ln(\frac{1}{2}\alpha\delta) - \pi i](\frac{1}{2}\alpha\delta)^2 - (3\gamma - \frac{13}{4} - \frac{3}{2}\pi i)(\frac{1}{2}\alpha\delta)^4}{-1 + [2\gamma + 2\ln(\frac{1}{2}\alpha\delta) - \pi i - 2](\frac{1}{2}\alpha\delta)^2} \qquad \text{(A10)}$$

Then, with $\delta = (\Omega^2 - K^2)^{1/2}$ and $n = 1$, (3.4) becomes

$$F(K, \Omega) = (\Omega^2 - 1)\,\delta^4 X^2 + \Omega^2(\delta^2 - 1)\,Y^2 - (2\Omega^2 - 1)\,\delta^2(\delta^2 - 1)XY - K^2 = 0 . \qquad \text{(A11)}$$

Inserting (A10) into (A11), multiplying out the terms, and keeping only those of order up to δ^2, result in the equation

$$(1 + X) + \Omega^2\{\alpha^2[2\gamma + 2\ln(\tfrac{1}{2}\alpha\delta) - \pi i - 1] - 2(1 + X)\}. \qquad \text{(A12)}$$

If δ is real, i.e., $\Omega > K$, the term $\ln(\frac{1}{2}\alpha\delta)$ is real and consequently (A12) is a complex equation. However, when $K > \Omega$, δ is imaginary since we have $\delta \equiv (\Omega^2 - K^2)^{1/2}$. This can be represented by $\delta = i\delta^* = e^{i\pi/2}\delta^*$ where δ^* is real, such that the natural logarithm becomes

$$\ln(\tfrac{1}{2}\alpha\delta) = \ln(\tfrac{1}{2}\alpha\delta^*) + \tfrac{1}{2}i\pi. \qquad \text{(A13)}$$

Thus (A12) is a real equation:

$$(1 + X) + \Omega^2\{\alpha^2[2\gamma + 2\ln(\tfrac{1}{2}\alpha\delta^*) - 1] - 2(1 + X)\} = 0 . \qquad \text{(A14)}$$

Moreover, the nature of the modes has finally been determined—virtual and radiative for $\Omega > K$, and real and nonradiative for $K > \Omega$. Consequently, $F(K, \Omega)$ is not continuous across the photon line and should approach it asymptotically for $K \approx \Omega$, $K > \Omega$. This latter point can be shown by giving

values to α and δ^* in (A14), i.e., for $\alpha = 1.0$ and $\delta^* = e^{-5} = 0.006738$ we have $\Omega = 0.390214$, while for $\alpha = 1.0$ and $\delta^* = e^{-10} = 0.0000454$, $\Omega = 0.301083$. Another computation, but this time with $\alpha = 0.1$, gave $\Omega = 0.695524$ for $\delta^* = e^{-5}$ and $\Omega = 0.687272$ for $\delta^* = e^{-10}$. The values of the modified Bessel functions in Watson[12] were used to compute X for both values of α.

[1]R. H. Ritchie, Phys. Rev. 106, 874 (1957).

[2]H. Raether in *Springer Tracts in Modern Physics*, edited by G. Hohler (Springer, New York, 1965), Vol. 38, p. 84.

[3]W. Steinmann, Phys. Status Solidi 28, 437 (1968).

[4]R. H. Ritchie, Surf. Sci. 34, 1 (1973).

[5]E. N. Economou and K. L. Ngai, Advances of Chemical Physics, edited by I. Prigogine and S. A. Rice (to be published).

[6]H. Jensen, Z. Phys. 106, 620 (1937); J. Crowell and R. H. Ritchie, Phys. Rev. 172, 436 (1968); Th. Kokkinakis and K. Alexopoulos, Phys. Rev. Lett. 28, 1632 (1972); for a review of the recent work see Ref. 5.

[7]R. Englman and R. Ruppin, J. Phys. C 1, 1515 (1968).

[8]C. Miziumski, Phys. Lett. A 40, 187 (1972).

[9]K. L. Ngai and E. N. Economou, Conference on Surface Properties and Surface States of Electronic Materials, Rolla, Mo., 1972 (unpublished).

[10]J. C. Ashley and L. C. Emerson, Surf. Sci. 41, 615 (1974).

[11]J. A. Stratton, *Electromagnetic Theory* (McGraw-Hill, New York, 1941).

[12]G. N. Watson, *A Treatise on the Theory of Bessel Functions*, 2nd ed. (Cambridge U. P., New York, 1962).

[13]M. Goldstein and R. M. Thaler, Math. Comput. 8, No. 66, (1959).

[14]J. C. Ashley and R. H. Ritchie have considered theoretically the problem of double bulk plasmon production, Phys. Status Solidi 38, 425 (1970).